Journal of Materials Chemistry

Cite this: J. Mater. Chem., 2012, 22, 3764

www.rsc.org/materials

PAPER

Facile and controllable one-pot synthesis of an ordered nanostructure of $Co(OH)_2$ nanosheets and their modification by oxidation for high-performance lithium-ion batteries

Xiao-lei Huang,†[ab] Xue Zhao,†[ac] Zhong-li Wang,[a] Li-min Wang[a] and Xin-bo Zhang*[a]

Received 23rd November 2011, Accepted 5th January 2012
DOI: 10.1039/c2jm16109e

Hybrids of $Co(OH)_2$ nanosheets (NSs) and Co_3O_4 nanoparticles (NPs) are synthesized by a facile hydrothermal strategy, wherein the $Co(OH)_2$ NSs form a flower-like structure and the Co_3O_4 NPs are embedded on the interlayer surfaces of the $Co(OH)_2$ NSs. The morphology, microstructure and composition of the hybrid can be tuned by the reaction time. When tested as anode materials for lithium-ion batteries, these ordered hybrid nanostructures of $Co(OH)_2$ NSs/Co_3O_4 NPs manifest significantly enhanced Li storage properties, including a high reversible capacity, long cycle life, and superior rate performance. The obtained promising performance could be attributed to the unique microstructure and the synergistic effect of the corresponding chemical composition in the nanocomposite.

1. Introduction

Lithium-ion batteries (LIBs) have been considered as a promising power source for electronic applications such as electric vehicles, laptop computers and mobile phones.[1,2] They are also intensively pursued for hybrid electric vehicles (HEV) and plug-in hybrid electric vehicles (PHEV).[3,4] Graphite, the anode material currently used in commercial LIBs, has a relatively low Li storage capacity. Thus there is a general consensus that a breakthrough in capacity requires passage from classical intercalation reactions to conversion reactions.[2,4–6] However even after decades of intensive efforts, capacity degradation and poor rate performance still seriously hamper the application of conversion-based materials.[2,4,6]

Nanostructured materials as the anode materials in LIBs have attracted intensive interest owing to their high specific surface areas and short lithium-ion transport paths.[7–12] As the morphology and microstructure have a substantial influence on the performance of materials even with the same composition, considerable efforts have been devoted to synthesize a variety of nanomaterials with different shapes and unique structures including nanoparticles,[13] nanowires,[14] nanotubes,[15] nanorods,[16] and even hierarchical nanoflowers[11,17] or more complex structures.[18] Cobalt hydroxide [$Co(OH)_2$] has recently received increasing attention due to its important technological applications in the field of catalysis,[19] magnetic materials,[20] electrochemical capacitors,[21] and as a promising conversion-based anode material for LIBs due to its high capacity.[22] Since $Co(OH)_2$ with a sheet-like structure tends to form a layered assembly,[23a] and thus has the benefit of improved ion transport and contact between electroactive materials and the electrolyte, several methods have been applied to synthesize sheet-like structured $Co(OH)_2$.[23] Dong *et al.* synthesized hexagonal β-$Co(OH)_2$ NSs by a facile hydrothermal synthetic method.[23a] Hou *et al.* also synthesized β-$Co(OH)_2$ NSs by homogeneous precipitation with sodium hydroxide as the alkaline reagent in the presence of poly(vinylpyrrolidone).[23b] Despite these successes, pure $Co(OH)_2$ NSs acting as an anode material still do not exhibit good cycling performance for LIBs,[22] which may be due to intrinsically large volume expansion, NS stacking and the insufficient soaking of electrolyte between layers during the cycling process. To solve this problem, construction of a $Co(OH)_2$ NS/Co_3O_4 NP hierarchical structure wherein the $Co(OH)_2$ NSs are sandwiched by Co_3O_4 NPs, could effectively keep the NSs separated and thus not only prevent the layers from stacking together but also provide efficient space for ion infiltration.

Herein, we proposed a facile and controllable one-pot synthesis of an ordered $Co(OH)_2$ NS/Co_3O_4 NP hierarchical structure, wherein the Co_3O_4 NPs are formed *in situ* by hydrothermal oxidation of the $Co(OH)_2$. In this structure, the Co_3O_4 NPs are closely embedded on the inter-layer surface of the $Co(OH)_2$, which could prevent the $Co(OH)_2$ nanosheets from

[a]*State Key Laboratory of Rare Earth Resource Utilization, Changchun Institute of Applied Chemistry, Chinese Academy of Sciences, Changchun, 130022, China. E-mail: xbzhang@ciac.jl.cn; Fax: +86-431-85262235; Tel: +86-431-85262235*
[b]*Graduate University of Chinese Academy of Sciences, Beijing, 100049, China*
[c]*Key Laboratory of Automobile Materials, Ministry of Education, School of Materials Science and Engineering, Jilin University, Changchun, 130012, China*
† Xiao-lei Huang and Xue Zhao contributed equally to this work.

stacking and buffer the local volume changes during cycling. Meanwhile, this structure enables a significant reduction of the Li^+ diffusion path and thus can expedite the ion transport. When applied as the anode material for LIBs, the as-prepared ordered hierarchical structured materials exhibit greatly enhanced Li storage properties, including a high reversible capacity, long cycle life, and superior rate performance.

2. Experimental sections

Materials

Cobalt nitrate hexahydrate ($Co(NO_3)_2 \cdot 6H_2O$, Aladdin Reagent, AR), ammonia solution (NH_4OH, 25%, Aladdin Reagent, AR), ethylene glycol ($C_2H_6O_2$, Aladdin Reagent, GR), methanol (CH_3OH, Aladdin Reagent, AR), acetylene black (MTI Corporation), polyvinylidenefluoride (PVDF, DuPont Company, 99.9%), *N*-methyl-2-pyrrolidinone (NMP, Aladdin Reagent, AR), separator (polypropylene film, Celgard 2400), electrolyte (1 M $LiPF_6$ in ethylene carbonate (EC)/dimethyl carbonate (DMC) with the weight ratio of 1 : 1, Zhangjiagang Guotai-Huarong New Chemical Materials Co., Ltd).

Preparation of $Co(OH)_2$ ordered structure

0.8731 g of $Co(NO_3)_2 \cdot 6H_2O$ was dissolved in 40 mL of deionized water, and then 1 mL of concentrated ammonia solution (25%) was slowly added into this solution. A blue flocculent precipitate was produced. After stirring 15 min for good dispersion, the precipitate was washed with deionized water three times. The fresh precipitate was dispersed in 40 mL of ethylene glycol, and the resulting mixture was transferred into a Teflon-lined autoclave (50 mL). The autoclave was sealed and heated to 180 °C and maintained this temperature for 48 h. The system was then naturally cooled to ambient temperature. The final product was filtered with a microfiltration membrane (pore size = 0.45 μm) and washed with distilled water three times.

Preparation of $Co(OH)_2/Co_3O_4$ hybrids

1.7462 g of $Co(NO_3)_2 \cdot 6H_2O$ was dissolved in 40 mL of deionized water, then the precursor precipitate was prepared by applying the above method. After that the fresh precipitate was dispersed in 20 mL of deionized water together with 20 mL of methanol, and then the resulting mixture was transferred into a Teflon-lined autoclave (50 mL). The autoclave was sealed and heated to 180 °C and maintained this temperature for 12 h, 72 h or 84 h. The system was then naturally cooled to ambient temperature. The final product was filtered with microfiltration membrane (pore size = 0.45 μm) and washed with distilled water three times.

Characterization methods

Powder X-ray diffraction (XRD) measurements were performed using a Rigaku-Dmax 2500 diffractometer with Cu Kα radiation (λ = 1.5405 Å). Scanning electron microscopy (SEM) was performed on a field emission Hitachi S-4800 instrument, operating at an accelerating voltage of 10 kV. Transmission electron microscopy (TEM) was performed using an FEI Tecnai G2 S-Twin instrument with a field emission gun operating at 200 kV to investigate the morphology of the as-prepared samples. Samples were dispersed in ethanol, then applied onto the copper grid with carbon coated on Lacey support film and dried in air before TEM imaging. X-Ray photoelectron spectrometry (XPS) data was acquired using an ESCALABMKLL X-ray photoelectron spectrometer with monochromatic Al Kα X-rays. Base pressure in the analysis chamber was 5.0×10^{-9} mbar.

Electrochemical measurement

The electrochemical experiments were performed *via* CR2025 coin-type test cells assembled in a dry argon-filled glove box in which both moisture and oxygen contents were below 1 ppm. The test cell consisted of a working electrode and a lithium foil which were separated by a Celgard 2400 membrane. The electrolyte solution was prepared by dissolving 1 M $LiPF_6$ in EC–DMC (1 : 1 w/w). The working electrodes were prepared by casting slurry containing 80% of active material, 10% of acetylene black and 10% of PVDF onto a copper foil. After vacuum drying at 80 °C for about 24 h, the electrode disks (d = 12 mm) were punched and weighed. Each electrode had *ca.* 3 mg of active material. Galvanostatic charge–discharge cycling tests were performed using an LAND CT2001A multi-channel battery testing system in the voltage range between 0.01 and 3 V at room temperature.

3. Results and discussion

The formation procedure of $Co(OH)_2/Co_3O_4$ ordered hierarchical structures is illustrated in Fig. 1a. Briefly, the precursor of this structure is obtained *via* the chemical reaction between $Co(NO_3)_2 \cdot 6H_2O$ and concentrated ammonia solution. The morphology of the precursor before hydrothermal treatment is an ordered sheet-like unit (Fig. 1b). After heating for a certain time *via* the hydrothermal method, the ordered flower-like structure is maintained (Fig. 1a), wherein Co_3O_4 NPs are closely anchored on the inter-layer surface of $Co(OH)_2$ NSs. Although there are some free NSs that are not in flower-like form, they still contain particles between the layers. However, when a certain

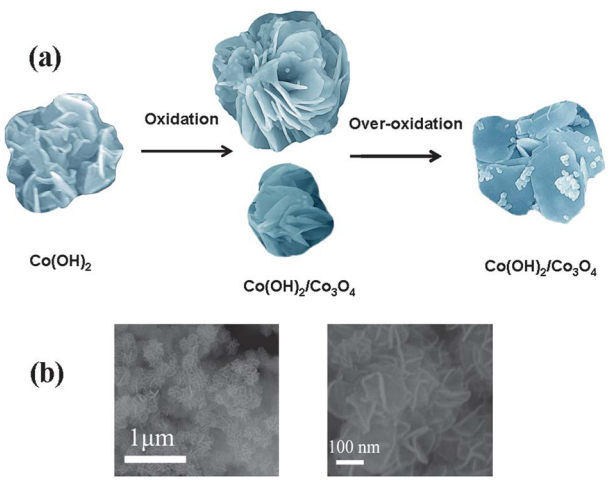

Fig. 1 (a) Schematic diagram of the formation procedures of the $Co(OH)_2/Co_3O_4$ ordered nanostructure, and (b) the morphology of the precursor.

time of oxidization is exceeded, the ordered nanostructure disappears accompanied by a restacking of the layers and agglomeration of the small particles. The X-ray diffraction patterns of the as-prepared $Co(OH)_2$ precursors and hydrothermal products of the 12 h, 72 h, and 84 h reaction times are shown in Fig. 2a–d, respectively. All the identified diffraction peaks in Fig. 2a can be unambiguously assigned to the phase-pure rhombohedral $Co(OH)_2$ (JCPDS No. 30–0443).[10] With an increase of the heating time, the precursor is partially oxidized to Co_3O_4, which can be clearly seen in Fig. 2b–d. The diffraction peaks at 2θ of 31.2° and 36.8° can be ascribed to well-crystallized Co_3O_4 with a face-centered cubic (fcc, *Fd3m* (227), $a = 0.808$ nm) structure (JCPDS No. 42–1467).[24] These results indicate that the composite consists of $Co(OH)_2$ NSs and well-crystallized Co_3O_4. Even after 84 h of heating, the $Co(OH)_2$ NSs haven't fully oxidized to Co_3O_4, and the composite of $Co(OH)_2/Co_3O_4$ is maintained. It is clear that the relative intensity of the Co_3O_4 diffraction peaks becomes stronger from Fig. 2b–d, indicating that the amount of Co_3O_4 increases with the extension of the hydrothermal reaction time.

Fig. 3 shows SEM images of the obtained products. The morphology of $Co(OH)_2$ NSs is shown in Fig. 3a, from which it is clearly observed that the $Co(OH)_2$ NSs are well scattered and almost no stacked layers can be found. Fig. 3b and c show the SEM images of the as-prepared $Co(OH)_2/Co_3O_4$ composite, from which it can be seen that the $Co(OH)_2$ NSs exhibit a flower-like structure, while the Co_3O_4 NPs with a size of 50–70 nm are evenly embedded on the inter-layer surface of the thin $Co(OH)_2$ layers. Also, some free $Co(OH)_2$ NSs are observed, which have small Co_3O_4 NPs closely anchored on their surface. When the heating time is prolonged to 84 h, the morphology of the as-prepared $Co(OH)_2/Co_3O_4$ composite changes dramatically (Fig. 3d). It is clearly observed that the ordered nanostructure has disappeared and the NSs are exfoliated and stacked, meanwhile the Co_3O_4 NPs have detached from the $Co(OH)_2$ NSs surfaces to agglomerate into large particles. The variation in miscrostructure of the $Co(OH)_2/Co_3O_4$ composites will thereafter influence their electrochemical performance (*vide infra*).

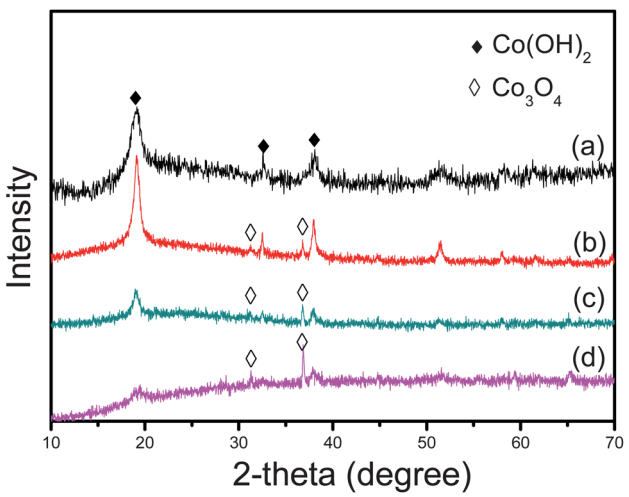

Fig. 2 The XRD patterns of $Co(OH)_2$ (a) and $Co(OH)_2/Co_3O_4$ hybrids with a hydrothermal reaction time of 12 h (b), 72 h (c), and 84 h (d).

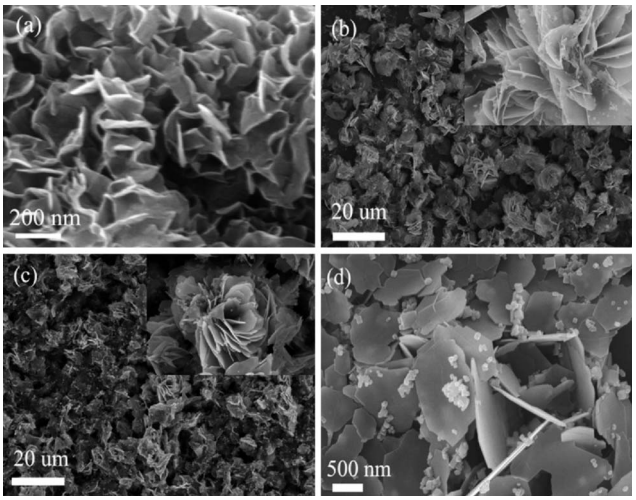

Fig. 3 SEM images of $Co(OH)_2$ (a) and $Co(OH)_2/Co_3O_4$ hybrids with a hydrothermal reaction time of 12 h (b), 72 h (c), and 84 h (d).

Further insight into the morphology and microstructure of the composite with a hydrothermal reaction time of 72 h is gained by using transmission electron microscopy (TEM). Fig. 4a is taken from the up layer of the flower-like structure. It shows that the small Co_3O_4 NPs are accompanied by the $Co(OH)_2$ NSs, where the dark square feature is a Co_3O_4 NP and the lower layer is the $Co(OH)_2$ NS. To confirm the phases of $Co(OH)_2$ and Co_3O_4, high resolution TEM is used (Fig. 4b and c). From the magnified image (Fig. 4b), the measured lattice spacings of 2.42 and 2.36 Å are in good agreement with the lattice spacings of the (311) ($d = 2.43$ Å) and (222) ($d = 2.34$ Å) planes of Co_3O_4, respectively. Fig. 4c taken from the edge of Fig. 4a indicates that the NS

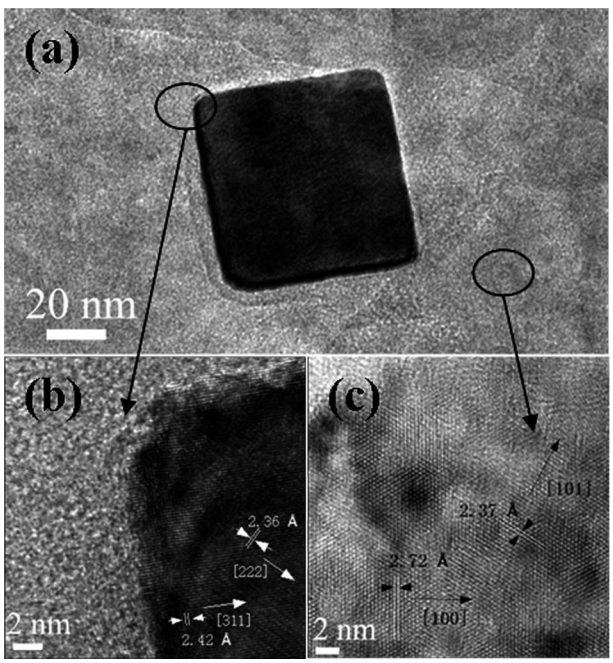

Fig. 4 The TEM images (a–c) of $Co(OH)_2/Co_3O_4$ hybrids with a hydrothermal reaction time of 72 h.

is a $Co(OH)_2$ phase, as the measured lattice spacings of 2.37 and 2.72 Å are congruent to the lattice spacings of the (101) (d = 2.37 Å) and (100) (d = 2.75 Å) planes of $Co(OH)_2$, respectively. The chemical constituents identified by TEM are consistent with the XRD results.

To obtain the relative content of $Co(OH)_2$ and Co_3O_4, a high-resolution XPS spectrum was employed (Fig. 5). As the Co $2p_{3/2}$ spectrum of $Co(OH)_2$ and Co_3O_4 can't be distinguished between 782.0 and 792.0 eV due to significant overlaps in binding energy, in this study, only the main characteristic peaks at about 780.7 and 779.9 eV for $Co(OH)_2$ and Co_3O_4, respectively, are curve-fitted.[25] The ratio of the main peak area of $Co(OH)_2$ and Co_3O_4 is used to analyze the relative content by the principle of component analysis from the curve-fitted spectrum. This can provide quantitative results for $Co(OH)_2$ and Co_3O_4 despite significant overlaps in binding energy. The main peak area ratios of $Co(OH)_2/Co_3O_4$ in Fig. 5a, b, and c are 1 : 0.25, 1 : 0.36, and 1 : 0.43, therefore, the content of Co_3O_4 is about 17.7, 23.7, and 27.1 wt% in the as-obtained $Co(OH)_2/Co_3O_4$, respectively, which increases with the heating time, in good agreement with the XRD results.

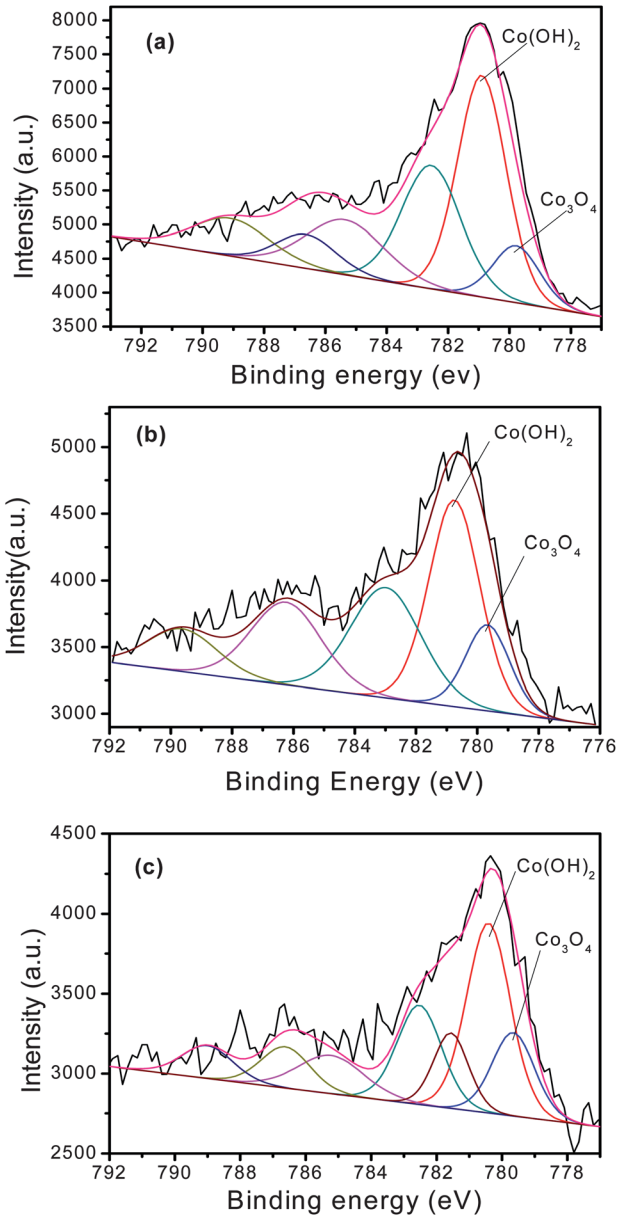

Fig. 5 XPS spectrum of as-obtained $Co(OH)_2/Co_3O_4$ hybrids with a hydrothermal reaction time of 12 h (a), 72 h (b), and 84 h (c).

The electrochemical properties of the bare $Co(OH)_2$ NSs and the $Co(OH)_2/Co_3O_4$ hybrids acting as anode materials were investigated in the voltage range between 0.01 and 3 V. The discharge–charge curves are shown in Fig. 6. It can be seen that these nanocomposites can have initial discharge/charge capacities of 961/581, 1412/905, 1452/1066, 1238/918 mA h g^{-1} at the first cycle, corresponding to coulombic efficiencies of about 63.08, 64.09, 73.42, and 74.15%, respectively (Fig. 6a–d). At the second cycle, these reversible capacities can be preserved at about 635, 901, 1128, and 954 mA h g^{-1}. The reversible capacities after 40 cycles are 98, 19, 1160, and 503 mA h g^{-1}, corresponding to 10.64, 1.34, 79.89, and 40.63% capacity retention of their initial values, respectively. Fig. 6c demonstrates the superior reversible capacity of the composite after heating for 72 h. This can be attributed to its unique hybrid structure of $Co(OH)_2/Co_3O_4$, wherein the small Co_3O_4 NPs embedded on the inter-layer surface of the thin $Co(OH)_2$ layers can effectively prevent volume expansion during the discharge–charge processes. Fig. 7 shows the rate capability and cycling performance of $Co(OH)_2$ and $Co(OH)_2/Co_3O_4$ hybrids with different hydrothermal reaction times. The $Co(OH)_2/Co_3O_4$ hybrids manifest a much better rate capability than that of a pure $Co(OH)_2$ electrode operated at various rates between 58 and 1160 mA g^{-1} (Fig. 7a). Among them, the composite with a hydrothermal reaction time of 72 h exhibits the best rate capability. Typically, it shows the highest capacities at different current densities compared to the other three electrodes during 50 cycles, moreover, when the rate returns to the initial 58 mA g^{-1} after 50 cycles, the composite almost recovers its original capacity (1100 mA h g^{-1}). This improved rate performance of the $Co(OH)_2/Co_3O_4$ hybrid could be reasonably ascribed to its thin layered structure, which provides more active sites during charging–discharging processes

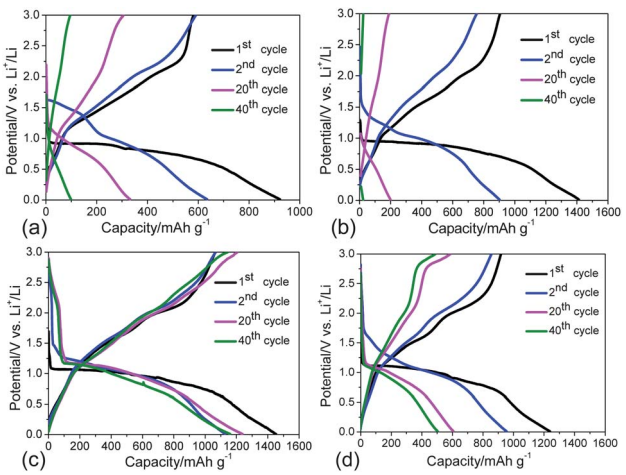

Fig. 6 (a) Discharge–charge profiles of pure $Co(OH)_2$ and $Co(OH)_2/Co_3O_4$ hybrids with different hydrothermal reaction times of 12 h (b), 72 h (c), and 84 h (d) at a current density of 58 mA g^{-1}.

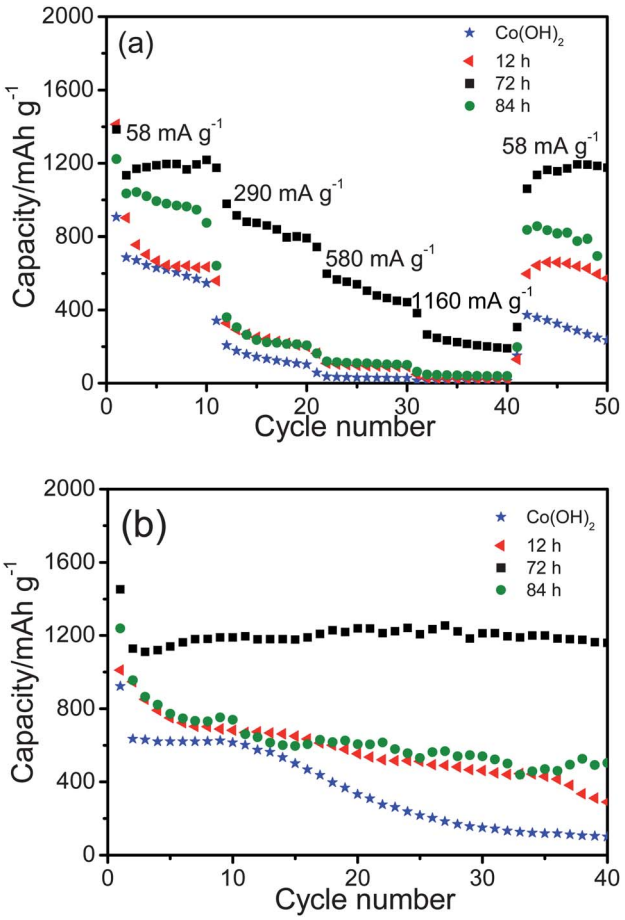

Fig. 7 (a) The rate capability and (b) cycling performance of $Co(OH)_2$/Co_3O_4 hybrids with different hydrothermal reaction times.

and faster ion transport. Fig. 7b depicts the cycling performance of the four samples up to 40 cycles. It is clear that the $Co(OH)_2$/Co_3O_4 hybrid that was heated for 72 h exhibits the highest capacity of more than 1100 mA h g^{-1}, even after 40 cycles, which is much higher than the theoretical capacity value of Co_3O_4 (890 mA h g^{-1}). The composites with a hydrothermal reaction time of 12 and 84 h show lower capacities during cycling, but they are still higher than that of pure $Co(OH)_2$. The rate performance in Fig. 7a also shows similar results. This is probably because the as-obtained $Co(OH)_2$ as an anode has poor electronic conductivity and undergoes large volume changes. The advantageous combination of $Co(OH)_2$ NSs and Co_3O_4 NPs, in addition to the flower-like structure, provides sufficient electrode/electrolyte contact area and facilitates continuous and fast diffusion paths for electrons through the electrodes during the lithiation/delithiation processes, endowing the $Co(OH)_2$/Co_3O_4 hybrid anode better electrochemical performance. This superior rate capability, reversible capacity and cycling performance can be reasonably attributed to synergistic effect of this unique structure—the *in situ* obtained Co_3O_4 NPs can not only prevent the aggregation of $Co(OH)_2$ NSs and buffer the intrinsic local volume change upon cycling, thus avoiding rapid fading of electrode capacity, but also provide void spaces for electrolyte infiltration and thus improve the rate capability.

4. Conclusions

In summary, we have demonstrated a facile and effective strategy to fabricate an ordered hybrid nanostructure of $Co(OH)_2$ NSs/Co_3O_4 NPs, wherein the morphology, microstructure and composition of the hybrid can be easily tuned by the reaction time. The obtained hierarchical structure could not only effectively buffer the intrinsic volume change but also provide a short ion transport pathway during cycling, thus leading to a significantly enhanced lithium-storage performance, including high reversible capacity, long cycling life, and good rate performance. The obtained promising results will certainly assist the long-term endeavours to develop high capacity anodes for rechargeable LIBs. We believe that the proposed strategy may be extended to other transition metal hydroxide materials, which can be used in broad fields including electrochemical capacitors and sensors.

Acknowledgements

This work is financially supported by the 100 Talents Programme of The Chinese Academy of Sciences, National Natural Science Foundation of China (Grant No. 21101147), and the Jilin Province Science and Technology Development Program (Grant No. 20100102 and 20116008).

Notes and references

1 (*a*) G. X. Wang, Y. Chen, K. Konstantinov, Jane Yao, Jung-ho Ahn, H. K. Liu and S. X. Dou, *J. Alloys Compd.*, 2002, **340**, L5; (*b*) Y. He, L. Huang, J. S. Cai, X. M. Zheng and S. G. Sun, *Electrochim. Acta*, 2010, **55**, 1140.
2 L. F. Cui, R. Ruffo, C. K. Chan, H. L. Peng and Y. Cui, *Nano Lett.*, 2009, **9**, 1491.
3 M. Armand and J. M. Tarascon, *Nature*, 2008, **451**, 652.
4 L. Ji, Z. K. Tan, T. R. Kuykendall, S. Aloni, S. D. Xun, E. Lin, V. Battaglia and Y. G. Zhang, *Phys. Chem. Chem. Phys.*, 2011, **13**, 7170.
5 W. Gruner, J. Thomas and L. Giebeler, *Electrode materials*, 2011, 12.
6 J. Cabana, L. Monconduit, D. Larcher and M. R. Palacin, *Adv. Mater.*, 2010, **22**, E170.
7 H. K. Liu, G. X. Wang, Z. P. Guo, J. Z. Wang and K. Kosta, *J. Nanosci. Nanotechnol.*, 2006, **6**, 1.
8 P. G. Bruce, B. Scrosati and J. M. Tarascon, *Angew. Chem., Int. Ed.*, 2008, **47**, 2930.
9 Y. Wang and G. Z. Cao, *IEEE Nanotechnol. Mag.*, 2009, **3**, 14.
10 C. H. Xu, J. Sun and L. Gao, *CrystEngComm*, 2011, **13**, 1586.
11 L. X. Yang, Y. J. Zhu, L. Li, L. Zhang, H. Tong, W. W. Wang, G. F. Cheng and J. F. Zhu, *Eur. J. Inorg. Chem.*, 2006, 4787.
12 (*a*) X. P. Gao, J. L. Bao, G. L. Pan, H. Y. Zhu, P. X. Huang, F. Wu and D. Y. Song, *J. Phys. Chem. B*, 2004, **108**, 5547; (*b*) I. Moriguchi, R. Hidaka, H. Yamada, T. Kudo, H. Murakami and N. Nakashima, *Adv. Mater.*, 2006, **18**, 69.
13 (*a*) U. Kasavajjula, C. S. Wang and A. J. Appleby, *J. Power Sources*, 2007, **163**, 1003; (*b*) J. H. Ryu, J. W. Kim, Y. E. Sung and S. M. Oh, *Electrochem. Solid-State Lett.*, 2004, **7**, A306; (*c*) I. S. Kim and P. N. Kumta, *J. Power Sources*, 2004, **136**, 145.
14 (*a*) K. T. Nam, D. W. Kim, P. J. Yoo, C. Y. Chiang, N. Meethong, P. T. Hammond, Y. M. Chiang and A. M. Belcher, *Science*, 2006, **312**, 885; (*b*) K. M. Shaju, F. Jiao, A. Debart and P. G. Bruce, *Phys. Chem. Chem. Phys.*, 2007, **9**, 1837; (*c*) M. S. Park, G. X. Wang, Y. M. Kang, D. Wexler, S. X. Dou and H. K. Liu, *Angew. Chem., Int. Ed.*, 2007, **46**, 750; (*d*) G. Armstrong, A. R. Armstrong, P. G. Bruce, P. Reale and B. Scrosati, *Adv. Mater.*, 2006, **18**, 2597; (*e*) D. K. Kim, P. Muralidharan, H. W. Lee, R. Ruffo, Y. Yang, C. K. Chan, H. L. Peng, R. A. Huggins and Y. Cui, *Nano Lett.*, 2008, **8**, 3948; (*f*) Y. G. Li, B. Tan and Y. Y. Wu, *Nano Lett.*, 2008, **8**, 265; (*g*) X. W. Lou, D. Deng, J. Y. Lee, J. Feng and L. A. Archer, *Adv. Mater.*, 2008, **20**, 258.

15 (*a*) J. Goldberger, R. He, Y. F. Zhang, S. Lee, H. Yan, H. J. Choi and P. D. Yang, *Nature*, 2003, **422**, 599; (*b*) J. Hu, Y. Bando, Z. Liu, J. Zhan, D. Golberg and T. Sekiguchi, *Angew. Chem., Int. Ed.*, 2004, **43**, 63; (*c*) Z. Liu, D. Zhang, S. Han, C. Li, B. Lei, W. Lu, J. Fang and C. Zhou, *J. Am. Chem. Soc.*, 2005, **127**, 6; (*d*) H. J. Fan, M. Knez, R. Scholz, K. Nielsch, E. Pippel, D. Hesse, M. Zacharias and U. Gosele, *Nat. Mater.*, 2006, **5**, 627.

16 (*a*) C. Wang, Y. L. Hou, J. M. Kim and S. H. Sun, *Angew. Chem., Int. Ed.*, 2007, **46**, 6333; (*b*) Q. Zhang, X. Y. Chen, Y. X. Zhou, G. B. Zhang and S. H. Yu, *J. Phys. Chem. C*, 2007, **111**, 3927; (*c*) T. S. Sreeprasad, A. K. Samal and T. Pradeep, *Langmuir*, 2007, **23**, 9463; (*d*) X. P. Gao, J. L. Bao, G. L. Pan, H. Y. Zhu, P. X. Huang, F. Wu and D. Y. Song, *J. Phys. Chem. B*, 2004, **108**, 5547.

17 (*a*) M. H. Cao, X. Y. He, J. Chen and C. W. Hu, *Cryst. Growth Des.*, 2007, **7**, 170; (*b*) H. Zhang, D. R. Yang, Y. J. Ji, X. Y. Ma, J. Xu and D. L. Que, *J. Phys. Chem. B*, 2004, **108**, 3955.

18 (*a*) X. C. Song, Y. Zhao, Y. F. Zheng, E. Yang and Z. S. Liu, *Sci. China Chem.*, 2010, **53**, 841; (*b*) B. X. Wang, H. Lin and Z. G. Yin, *Mater. Lett.*, 2011, **65**, 41; (*c*) J. S. Chen, T. Zhu, Q. H. Hu, J. J. Gao, F. B. Su, S. Z. Qiao and X. W. Lou, *ACS Appl. Mater. Interfaces*, 2010, **2**, 3628.

19 (*a*) M. Dinamani and P. V. Kamath, *J. Appl. Electrochem.*, 2000, **30**, 1157; (*b*) T. L. Lai, Y. L. Lai, C. C. Lee, Y. Y. Shu and C. B. Wang, *Catal. Today*, 2008, **131**, 105; (*c*) L. F. Fan, X. Q. Wu, M. D. Guo and Y. T. Gao, *Electrochim. Acta*, 2007, **52**, 3654.

20 (*a*) L. Li, H. Qian and J. Ren, *Chem. Commun.*, 2005, 4083; (*b*) M. Kurmoo, *Chem. Mater.*, 1999, **11**, 3370.

21 Y. S. He, D. W. Bai, X. Yang, J. Chen, X. Z. Liao and Z. F. Ma, *Electrochem. Commun.*, 2010, **12**, 570.

22 (*a*) L. Cao, F. Xu, Y. Y. Liang and H. L. Li, *Adv. Mater.*, 2004, **16**, 1853; (*b*) W. J. Zhou, J. Zhang, T. Xue, D. D. Zhao and H. L. Li, *J. Mater. Chem.*, 2008, **18**, 905; (*c*) C. Yuan, L. Hou, L. Shen, D. Li, F. Zhang, C. Fan, J. Li and X. Zhang, *Electrochim. Acta*, 2010, **56**, 115; (*d*) J. K. Chang, C. M. Wu and I. W. Sun, *J. Mater. Chem.*, 2010, **20**, 3729.

23 (*a*) Q. Dong, N. Kumada, Y. Yonesaki, T. Takei and N. Kinomura, *Mater. Res. Bull.*, 2011, **46**, 1156; (*b*) Y. Hou, H. Kondoh, M. Shimojo, T. Kogure and T. Ohta, *J. Phys. Chem. B*, 2005, **109**, 19094.

24 Y. Li, L. N. Xu and J. Chen, *Adv. Funct. Mater.*, 2005, **15**, 851.

25 J. Yang, H. W. Liu, W. N. Martens and R. L. Frost, *J. Phys. Chem. C*, 2010, **114**, 111.